


RESEARCH ARTICLE

Open Access



Synthesis and validation of [^{18}F]mBPET-1, a fluorine-18 labelled mTOR inhibitor derivative based on a benzofuran backbone

Christian W. Wichmann^{1,2,3,4*} , Yit Wooi Goh², Adam C. Parslow^{3,4}, Angela Rigopoulos^{3,4}, Nancy Guo³, Andrew M. Scott^{1,2,3,4}, Uwe Ackermann^{1,2,3,4} and Jonathan M. White¹

* Correspondence: christian.wichmann@onjcri.org.au

¹The University of Melbourne, Parkville, VIC 3010, Australia

²Department of Molecular Imaging and Therapy, Austin Hospital, 145 Studley Road, Heidelberg, VIC 3084, Australia

Full list of author information is available at the end of the article

Abstract

Background: Targeted therapy of HER2 positive breast cancer has led to clinical success in some cases with primary and secondary resistance being major obstacles. Due to the substantial involvement of mTOR kinase in cell growth and proliferation pathways it is now targeted in combination treatments to counteract HER2 targeted therapy resistance. However, the selection of receptive patient populations for a specific drug combination is crucial. This work aims to develop a molecular probe capable of identifying patients with tumour populations which are receptive to RAD001 combination therapy. Based on the structure of a mTOR inhibitor specific for mTORC1, we designed, synthesised and characterised a novel benzofuran based molecular probe which suits late stage fluorination via Click chemistry.

Results: Synthesis of the alkyne precursor 5 proceeded in 27.5% yield over 7 linear steps. Click derivatisation gave the non-radioactive standard in 25% yield. Radiosynthesis of [^{18}F]1-((1-(2-Fluoroethyl)-1H-1,2,3-triazol-4-yl) methyl)-4-((5-methoxy-2-phenylbenzofuran-4-yl) methyl) piperazine ([^{18}F]mBPET-1) proceeded over two steps which were automated on an iPhase FlexLab synthesis module. In the first step, 2-[^{18}F]fluoroethylazide ([^{18}F]6) was produced, purified by automated distillation in 60% non-decay-corrected yield and subjected to Click conditions with 5. Semi-preparative RP-HPLC purification and reformulation gave [^{18}F]mBPET-1 in 40% \pm 5% ($n = 6$) overall RCY with a process time of 90 min. Radiochemical purity was $\geq 99\%$ at end of synthesis (EOS) and $\geq 98\%$ after 4 h at room temperature. Molar activities ranged from typically 24.8 GBq/ μmol (EOS) to a maximum of 78.6 GBq/ μmol (EOS). Lipophilicity of [^{18}F]mBPET-1 was determined at pH 7.4 ($\log D_{7.4} = 0.89$). [^{18}F]mBPET-1 showed high metabolic stability when incubated with mouse S9 liver fractions which resulted in a 0.8% drop in radiochemical purity after 3 h. Cell uptake assays showed 1.3–1.9-fold increased uptake of the [^{18}F]mBPET-1 in RAD001 sensitive compared to insensitive cells across a panel of 4 breast cancer cell lines.

Conclusion: Molecular targeting of mTOR with [^{18}F]mBPET-1 distinguishes mTOR inhibitor sensitive and insensitive cell lines. Future studies will explore the ability of [^{18}F]mBPET-1 to predict response to mTOR inhibitor treatment in in vivo models.

Keywords: Fluorine-18, ^{18}F , mTOR, Everolimus therapy, RAD001, PET, Molecular targeting, Breast cancer

Introduction

Inhibition of growth signalling receptors such as human epidermal growth factor receptor 2 (HER2) has shown some success in the treatment of breast cancer especially in patients with chemotherapy resistant metastatic disease (Baselga et al. 1996; Cobleigh et al. 1999). However, primary and secondary resistance to HER2 targeted therapies is a common problem among patient populations (Gajria and Chandarlapaty 2011; Narayan et al. 2009). The phosphatidylinositide 3-kinase (PI3K) pathway is a prominent oncogenic signalling pathway downstream of HER2 with the mammalian target of rapamycin (mTOR) as a key mediator (Bjornsti and Houghton 2004). mTOR protein forms a part of two distinct kinases, mTOR complex 1 and 2, which are heavily involved in cell growth and proliferation pathways (Tchevkina and Komelkov 2012). Due to its central role in oncogenesis, mTOR has become a popular target for cancer therapy and a number of mTOR targeted therapeutics have been developed (Liu et al. 2013; Vinayak and Carlson 2013; Wander et al. 2011; Yu et al. 2010; Zhou and Huang 2012). A growing number of preclinical and clinical trials now focus on inhibition of mTOR in combination with drugs targeting other growth signalling pathways such as HER2 (Gayle et al. 2012; Gnant 2013; Hurvitz et al. 2013; Jerusalem et al. 2011; Lu et al. 2007).

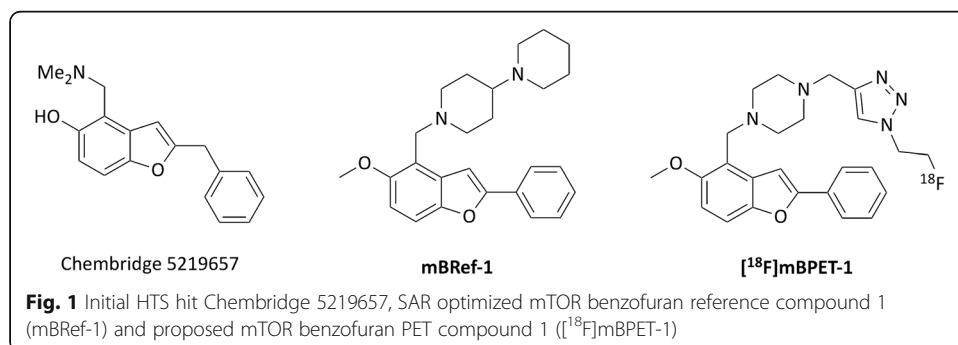
Everolimus (RAD001) is an mTOR complex 1 selective kinase inhibitor which has been approved as a chemotherapeutic for a number of indications such as renal cell carcinoma, neuroendocrine tumours and biliary as well as breast cancer (Baselga et al. 2011; Lau et al. 2018; Motzer et al. 2010; Yao et al. 2016).

Due to its wide applicability, RAD001 is gaining popularity as a combination drug. The TRINITY-1 study which examines triplet therapy of hormone receptor positive (HR+), HER2- advanced breast cancer with ribociclib (CDK4/6 inhibition), RAD001 (mTOR inhibition) and exemestane (endocrine therapy) showed clinical benefit in a preliminary analysis in 95 patients (Bardia et al. 2019). Combination of RAD001 with the HER2 targeting monoclonal antibody trastuzumab (Herceptin) is currently being investigated in clinical trials and has progressed to phase 3 (Andre et al. 2010; Hurvitz et al. 2013; Hurvitz et al. 2015a, 2015b; Jerusalem et al. 2011). The BOLERO-3 trial, which focusses on patients with trastuzumab-resistant advanced breast cancer, showed an improvement in median progression-free survival from 5.78 to 7.00 months in the RAD001 cohort compared to the placebo group (Andre et al. 2014). However, closer analysis of biomarker specific response showed that patients with low expression of phosphatase and tensin homolog (PTEN) or high levels of phospho-S6 kinase (pS6) exhibited better response to combination therapy with RAD001. Both low PTEN and high pS6 are indicators of mTOR activation. These results sparked the development of a molecular probe that would allow for the selection of responsive patient populations in a non-invasive manner using positron emission tomography (PET). PET is a non-invasive molecular imaging technique that is capable of visualising biological processes in living organisms. mTOR expression is typically determined via immunohistochemistry (IHC) of tumour biopsies, however these merely provide snapshots of the respective disease and results are highly sampling-dependent (Laes et al. 2017). Molecular imaging techniques can be complementary to biopsy (Adams et al. 2014; Fei and Schuster 2017) or provide advantages especially in the characterisation of deep soft-tissue, lymph node and visceral metastases (Krug et al. 2008).

Currently, there are no mTOR imaging probes for PET or SPECT under investigation in preclinical or clinical studies, neither can a description of the development of such a probe be found in the literature. Very recently, imaging of a related kinase which is part of the same cellular signalling pathway, PI3K, has been described (Altine et al. 2019; Han et al. 2019). In this work, Pictilisib (GDC-0941), a PI3K inhibitor, was radiolabelled with either carbon-11 or fluorine-18 to identify Pictilisib sensitive tumour populations.

In a similar fashion, it was hypothesised that the structure of a mTOR inhibitor could be used as a biological targeting vector to identify cells with high or low RAD001 sensitivity via their mTOR expression or activation levels. The design of the PET ligand was based on work by Salome et al. who have optimized the properties of a novel benzofuran based mTOR inhibitor (Salome et al. 2014a, 2014b). Chembridge 5219657 (Fig. 1) was identified in a high throughput screen (HTS) looking at molecules blocking the nuclear export of Forkhead box protein O1a, which is PI3K/AKT/mTOR pathway dependent (Kau et al. 2003). Salome et al. further characterised this class of compounds via a pull-down assay. Western blot analysis showed that the affigel-coupled derivate exclusively binds to mTOR, or an associated protein, but not to other kinases in the AKT/mTOR pathway. Treatment of SQ20B cancer cells with the benzofuran inhibitor showed dose dependent decrease of pS6 levels and delayed dose dependent increase of pAKT levels. Increased phosphorylation of AKT is a result of mTORC1 inhibition which reduces signalling through a negative feedback loop amplifying PI3K activity which leads to phosphorylation of AKT via PDK1 (Sabatini 2006). These findings were promising since RAD001 is selective for mTORC1.

Structural variations of Chembridge 5219657 identified the phenyl and the 2-phenoxybenzyl as the most potent substituents in the aryl position (Salome et al. 2014a). Modification of the benzofuran core to an indole, benzoxazole, furopyridine or benzimidazole had adverse effects on the cytotoxicity in SQ20B cancer cells. Modification of the amine substituent in 4-position showed the greatest variation in potency. Replacement of the dimethylamino-group with diethanolamine eliminated the target affinity. Alkylated piperazines were tolerated but surpassed by the 1,4'-bipiperidine and the 4-(dimethylamino)piperidine derivatives which proved to be the most favourable substituents. Attachment of a linker to the bipiperidine allowing for pull-down assays only resulted in a minor loss of potency. Based on these results, the radioligand was designed around a benzofuran core with fluorine-18 attached to a piperazine moiety in 4-position. Copper catalysed click chemistry is a proven method of introducing fluorine-18 in good radiochemical yields (Pretze et al. 2013). A fully automated



procedure has been developed which allows convenient derivatisation of alkyne precursors with 2- ^{18}F fluoroethylazide (Ackermann et al. 2014).

In conclusion, the most refined compound to date outperforms the initial structure identified by HTS by about two orders of magnitude and is close to 20-fold more cytotoxic than RAD001. Whether these numbers translate into mTORC1 affinity, however, remains an assumption due to the phenotypic nature of the assay used. Figure 1 shows mTOR benzofuran reference compound 1 (mBRef-1), one of the most potent derivatives of the series ($\text{IC}_{50} = 2.5 \mu\text{M}$). This structure was altered to give the proposed mTOR benzofuran PET compound 1 (^{18}F mBPET-1) which suits late-stage fluorination via click chemistry and enables its use in PET.

Experimental section

General methods

All chemicals and solvents were purchased from Sigma-Aldrich, Merck, Matrix Scientific, Combi-Blocks and AK Scientific and used as received unless stated otherwise. Analytical thin layer chromatography (TLC) was carried out using aluminium backed 2 mm thick Merck Kieselgel Silica gel 60 GF254 plates. Compounds were visualized under $\text{UV}_{254 \text{ nm}}$ light. Cartridges for solid phase extraction (SPE) of radioactive compounds were purchased from Waters and Phenomenex and conditioned with ethanol and washed with sterile water.

Automated flash chromatography was carried out on a Biotage Isolera One or a GRACE Reveleris system using Biotage SNAP or GRACE Flash cartridges. Semi-preparative reversed-phase high performance liquid chromatography (RP-HPLC) purification of organic molecules was performed on Agilent 1100, 1200 and 1260 series systems equipped with an automated sample injector, diode array UV-detector and automated fraction collector. Mass selective semi-preparative RP-HPLC purification was performed on a Shimadzu LC-20AR HPLC system equipped with a LCMS-2020 module and a FRC-10A fraction collector.

Nuclear magnetic resonance (NMR) spectra for ^1H , ^{13}C and ^{19}F nuclei were recorded at ambient temperature using an Agilent MR400 system with autosampler, Varian Unity Inova 500/600 or Bruker Avance III 600 NMR-spectrometers. NMR chemical shifts are reported in parts per million (ppm) and can be followed (in brackets) by multiplicity (s: singlet, d: doublet, t: triplet, m: multiplet, dd: doublet of doublets, dt: doublet of triplets), coupling constants (J) given in Hertz (Hz) and integration.

High-resolution mass spectrometry (HRMS) was performed on a Finnigan LTQ FT hybrid mass spectrometer (Bremen, Germany) linear ion trap with Fourier Transform Ion Cyclotron Resonance (FT-ICR) or on a Thermo Fisher Q Exactive Plus Hybrid Quadrupole-Orbitrap mass spectrometer in conjunction with a Thermo Fisher Ultimate 3000 UHPLC system equipped with an autosampler. Liquid chromatography mass spectrometry (LCMS) was carried out on an Agilent 1200 series RP-HPLC system with an Agilent 6220 Accurate-Mass TOF LC/MS system or on a Shimadzu LC20AD RP-HPLC system with a Shimadzu LCMS-2010 EV mass spectrometer. Gas chromatography-mass spectrometry (GCMS) was performed on an Agilent 7890A GC-system coupled to an Agilent 5975C MSD-module. Mass spectrometric data is

expressed as the mass to charge ratio (m/z) and is followed by relative intensities with respect to the base peak.

Analytical radio-HPLC was performed on a Shimadzu LC-20 AD gradient HPLC system equipped with a Shimadzu SPD-20A UV/VIS detector and a Bioscan Model 106 radio-HPLC flow-count detector. Semi-preparative RP-HPLC of radiolabelled compounds was performed on the iPHASE FlexLAB associated HPLC system using a Knauer HPLC pump.

Cell lines were obtained from American Type Culture Collection ATCC (Manassas, MD). Cell lines were cultured in RPMI media containing 10% FCS, 1% GlutaMAX (Gibco) and 1% Penicillin Streptomycin (Pen Strep, Gibco). Cells were maintained at 37 °C in humidified 5% CO₂ atmosphere. Cell number and viability determination was performed using trypan blue and a Bio-Rad TC20 automated cell counter. Radioactivity was determined using a Perkin Elmer Wizard2 gamma counter. Cell proliferation assays were performed using CellTiter 96[®] Aqueous One Solution (Promega, USA containing 3-(4,5-Dimethylthiazol-2-yl)-5-(3-carboxymethoxyphenyl)-2-(4-sulfophenyl)-2H-tetrazolium (MTS) reagent.

Chemistry

2-Bromo-1,4-dihydroxybenzene (1). Hydroquinone (10.00 g, 90.8 mmol, 1.00 eq) was dissolved in diethyl ether (100 mL). Bromine (14.51 g, 90.8 mmol, 4.65 mL, 1.00 eq) was added dropwise to the solution under cooling in an ice/water bath. The mixture was stirred at room temperature for 2 h. Subsequently, the mixture was quenched with 10% Na₂S₂O₃ solution (100 mL), extracted with diethyl ether (3 × 100 mL), washed with water (2 × 100 mL) and brine (100 mL), dried over MgSO₄ and the solvent was removed under vacuum. The product was isolated by automated flash chromatography using an isocratic solvent system and a Grace Reveleris 80 g silica cartridge. Removing the solvent under vacuum gave 1 as a white powder (13.70 g, 80%); Mp: 114.6–116.2 °C (lit. Reference (Akita 1962): 113–115 °C); ¹H-NMR (500 MHz, DMSO-d₆) δ 9.34 (s, 1H), 9.03 (s, 1H), 6.85 (d, J = 2.9 Hz, 1H), 6.75 (d, J = 8.8 Hz, 1H), 6.59 (dd, J = 8.8, 2.9 Hz, 1H); ¹³C-NMR (100 MHz, DMSO-d₆) δ 109.4, 115.8, 117.2, 119.3, 147.0, 150.9; Low-res. EI-MS calculated for C₆H₅BrO₂: 187.95 (100.0%), 189.95 (97.9%), 188.95 (6.6%), 190.95 (6.5%); Found: 187.9 (100.0%), 189.9 (89.1%), 188.9 (9.4%), 190.9 (6.6%).

2-Phenylbenzofuran-5-ol (2). 2-bromo-1,4-dihydroxybenzene (5.00 g, 26.45 mmol, 1.00 eq) and dry triethylamine (5.35 g, 52.91 mmol, 7.40 mL, 2.00 eq) were dissolved in dry THF (32 mL) and acetyl chloride (4.15 g, 52.91 mmol, 3.80 mL, 2.00 eq) was added dropwise at 0 °C. After stirring at room temperature for 5 min diisopropylamine (32 mL), palladium (II) acetate (296 mg, 1.32 mmol, 5 mol%), tri-tert-butylphosphonium tetrafluoroborate (574 mg, 1.98 mmol, 7.5 mol%), copper (I) iodide (251 mg, 1.32 mmol, 5 mol%) and phenylacetylene (5.40 g, 52.91 mmol, 5.80 mL, 2.00 eq) were added to the solution. The reaction was degassed using the freeze-pump-thaw method, heated to 60 °C and stirred for 2 h under nitrogen. Subsequently, methanol (106 mL) and potassium hydroxide (14.80 g, 264.54 mmol, 20.00 eq) in water (21 mL) were added and the solution was stirred at 75 °C for 2 h. After cooling to room temperature the mixture was neutralized with a 10% hydrochloric acid solution and extracted with dichloromethane (3 × 100 mL). The organic phase was washed with brine (150 mL), dried over

MgSO₄ and the solvent was removed under vacuum. Isolation by automated flash chromatography using an isocratic solvent system and a Grace Reveleris 80 g silica cartridge gave 2 as a yellow powder (5.31 g, 96%); Mp: 186.8–188.5 °C (lit. Reference (Alvey et al. 2008; Grinev et al. 1957): 186–186.5 °C or 191 °C); ¹H-NMR (500 MHz, DMSO-d₆) δ 9.20 (s, 1H), 7.85 (m, 2H), 7.47 (m, 2H), 7.39 (d, ³J = 8.8 Hz, 1H), 7.36 (m, 1H), 7.26 (d, ⁵J = 0.7 Hz, 1H), 6.93 (d, ⁴J = 2.4 Hz, 1H), 6.74 (dd, ³J = 8.8 Hz, ⁴J = 2.7 Hz, 1H); ¹³C-NMR (125 MHz, DMSO-d₆) δ 156.0, 154.0, 148.9, 130.4, 130.0, 129.4 (2), 129.1, 124.9 (2), 113.8, 111.8, 105.8, 102.4; Low-res. EI-MS calculated for C₁₄H₁₀O₂: 210.07 (100.0%), 211.07 (15.3%), 212.07 (1.5%); Found: 210.1 (100%), 211.1 (17.2%), 212.1 (1.8%).

5-hydroxy-2-phenylbenzofuran-4-carbaldehyde (3a). Paraformaldehyde (857 mg, 28.54 mmol, 6.0 eq), magnesium chloride (770 mg, 8.09 mmol, 1.7 eq) and triethylamine (9.51 mmol, 1.33 mL, 2.0 eq) were added to a stirred solution of 2-phenylbenzofuran-5-ol (1.00 g, 4.76 mmol, 1.0 eq) in acetonitrile (25 mL). The mixture was heated to reflux for 19 h and the yellow suspension was subsequently quenched with 10% aq. HCl (10 mL). The aqueous layer was extracted with EtOAc (3 × 30 mL). The combined organic layers were washed with water (50 mL), brine (50 mL), dried over MgSO₄ and the solvents were evaporated under reduced pressure to give the crude product as a brown solid. The product was isolated by automated flash chromatography to give 3a as bright yellow crystals (741 mg, 65%). Mp: 121.5–122.9 °C; ¹H-NMR (600 MHz, CDCl₃) δ 11.40 (s, 1H), 10.35 (d, ⁴J = 0.4 Hz, 1H), 7.87 (m, 2H), 7.64 (dd, ³J = 8.9 Hz, ⁵J = 0.7 Hz, 1H), 7.47 (m, 2H), 7.40 (tt, ³J = 7.4 Hz, ⁴J = 1.4 Hz, 1H), 7.30 (d, ⁵J = 0.9 Hz, 1H), 6.86 (dd, ³J = 8.9 Hz, ⁴J = 0.4 Hz, 1H); ¹³C-NMR (150 MHz, CDCl₃) δ 192.6, 159.8, 159.4, 148.8, 130.8, 129.6, 129.4, 128.9 (2), 125.2 (2), 120.2, 113.8, 111.4, 97.6; Low-res. EI-MS calculated for C₁₅H₁₀O₃: 238.06 (100.0%), 239.07 (16.5%), 240.07 (1.9%); Found: 238.1 (100.0%), 239.1 (16.4%), 240.1 (1.9%).

5-Methoxy-2-phenylbenzofuran-4-carbaldehyde (3b). Methyl iodide (523 μL, 8.39 mmol, 2.0 eq) and potassium carbonate (1.16 g, 8.39 mmol, 2.0 eq) were added to a solution of 5-methoxy-2-phenylbenzofuran (1.00 g, 4.20 mmol, 1.0 eq) in acetone (20 mL). The mixture was heated in a sealed tube at 55 °C for 18 h. The reaction was then cooled to room temperature and the solvent was removed under a stream of nitrogen. The residue was dissolved in water (50 mL) and extracted with dichloromethane (3 × 50 mL). The combined organic layers were washed with brine (100 mL), dried over MgSO₄ and the solvent was removed under vacuum which afforded 3b as a yellow powder (1.06 g, 99%). Mp: 106.5–110.3 °C; ¹H-NMR (600 MHz, CDCl₃) δ 10.64 (s, 1H), 7.90 (d, J = 7.3 Hz, 2H), 7.83 (s, 1H), 7.64 (d, J = 8.9 Hz, 1H), 7.45 (t, J = 7.6 Hz, 2H), 7.37 (t, J = 7.3 Hz, 1H), 6.90 (d, J = 8.8 Hz, 1H), 3.96 (s, 3H); ¹³C-NMR (150 MHz, CDCl₃) δ 190.3, 160.2, 160.0, 150.0, 130.0, 129.3, 129.3, 128.9 (2), 125.4 (2), 117.7, 116.6, 108.0, 102.6, 56.7; Low-res. EI-MS calculated for C₁₆H₁₂O₃: 252.08 (100.0%), 253.08 (17.6%), 254.09 (1.4%); Found: 252.1 (100.0%), 253.1 (17.3%), 254.1 (2.0%).

1-(Prop-2-yn-1-yl) piperazine (4). Propargyl bromide (1.19 g, 1.11 mL, 10.0 mmol, 1.00 eq) and piperazine (8.61 g, 100 mmol, 10.00 eq) were dissolved in THF (90 mL) and potassium carbonate (4.15 g, 30.0 mmol, 3.00 eq) was added. The reaction was stirred for 4 h under reflux. Subsequently, the solvent was removed under vacuum and the residue was dissolved in water (40 mL). The aqueous phase was extracted with ethyl acetate (4 × 40 mL), washed with brine (2 × 40 mL), dried over MgSO₄ and the solvent

was removed under vacuum to afford 4 as a light brown powder (174 mg, 14%); $^1\text{H-NMR}$ (500 MHz, CDCl_3) δ 3.28 (d, $J = 2.5$ Hz, 2H), 2.93 (t, $J = 4.9$ Hz, 4H), 2.65 (s, 1H), 2.54 (m, 4H), 2.25 (t, $J = 2.5$ Hz, 1H); $^{13}\text{C-NMR}$ (125 MHz, CDCl_3) δ 73.2, 53.1 (2), 51.7, 47.4, 46.0 (2); HRMS calculated for $\text{C}_7\text{H}_{13}\text{N}_2$ (MH^+): 125.10732; Found: 125.10734.

1-((5-Methoxy-2-phenylbenzofuran-4-yl) methyl)-4-(prop-2-yn-1-yl) piperazine (5). Catalytic acetic acid (2 drops), followed by sodium cyanoborohydride (50 mg, 0.79 mmol, 2.0 eq) was added to a stirred solution of 5-methoxy-2-phenylbenzofuran-4-carbaldehyde (100 mg, 0.40 mmol, 1.0 eq) and 1-(prop-2-yn-1-yl) piperazine (49 mg, 0.40 mmol, 1.0 eq) in methanol (10 mL). The mixture was stirred at room temperature for 18 h. The solvent was removed under vacuum and the product was isolated by automated flash chromatography to yield 5 as a yellow oil (78 mg, 55%); $^1\text{H-NMR}$ (500 MHz, CDCl_3) δ 7.88 (d, $J = 7.1$ Hz, 2H), 7.46 (t, $J = 7.7$ Hz, 2H), 7.36 (m, 2H), 7.25 (s, 1H), 6.91 (d, $J = 8.8$ Hz, 1H), 3.87 (s, 3H), 3.84 (s, 2H), 3.29 (d, $J = 2.4$ Hz, 2H), 2.62 (br. s., 8H), 2.24 (t, $J = 2.4$ Hz, 1H); $^{13}\text{C-NMR}$ (126 MHz, CDCl_3) δ 156.4, 154.1, 150.0, 130.9, 130.6, 128.7 (2), 128.5, 124.9 (2), 118.1, 110.0, 109.6, 101.4, 79.1, 73.0, 57.3, 53.8, 53.0 (2), 52.1 (2), 46.8; HRMS calculated for $\text{C}_{23}\text{H}_{25}\text{N}_2\text{O}_2$ (MH^+): 361.19105; Found: 361.18994.

2-Fluoroethylazide (6). Sodium azide (65 mg, 1.00 mmol) was added to a solution of 2-fluoroethyl 4-toluenesulfonate (218 mg, 1.00 mmol) in dimethylformamide (10 mL). The mixture was stirred for 24 h at room temperature and used for subsequent Click Chemistry reactions without further purification.

1-((1-(2-Fluoroethyl)-1H-1,2,3-triazol-4-yl) methyl)-4-((5-methoxy-2-phenylbenzofuran-4-yl) methyl) piperazine (mBPET-1). Copper (I) iodide (2.5 mg, 0.013 mmol, 10 mol%) and sodium ascorbate (26 mg, 0.13 mmol, 1.1 eq) were dissolved in water (250 μL). Subsequently, acetonitrile (250 μL), dimethylformamide (200 μL) and diisopropylethylamine (25 μL , 0.14 mmol, 1.2 eq) were added and mixed thoroughly to give a cloudy orange mixture. Freshly prepared 2-fluoroethylazide solution (1.2 mL, 0.12 mmol, 1.0 eq) was added to a stirred solution of 5 (30 mg, 0.12 mmol, 1.0 eq) in dimethylformamide (300 μL). The catalyst mixture was then added and the reaction was left to stir at room temperature for 2 h. Upon completion the reaction was concentrated under reduced pressure and extracted with ethyl acetate (3×3 mL). The combined organic phases were dried over MgSO_4 and the solvent was removed under reduced pressure to give a yellow oil. mBPET-1 was isolated by semi-preparative RP-HPLC and obtained as its TFA salt in the form of a white powder (20 mg, 25%); $^1\text{H-NMR}$ (600 MHz, CDCl_3) δ 7.90 (s, 1H), 7.87 (d, $J = 7.3$ Hz, 2H), 7.56 (d, $J = 8.8$ Hz, 1H), 7.46 (t, $J = 7.6$ Hz, 2H), 7.39 (t, $J = 7.4$ Hz, 1H), 7.21 (s, 1H), 6.91 (d, $J = 9.0$ Hz, 1H), 4.79 (dt, $^2J_{\text{HF}} = 46.6$ Hz, $^3J_{\text{HH}} = 4.7$ Hz, 2H), 4.68 (dt, $^3J_{\text{HF}} = 26.6$ Hz, $^3J_{\text{HH}} = 4.7$ Hz, 2H), 4.52 (s, 2H), 4.28 (s, 2H), 3.89 (s, 3H), 3.62 (br. s., 4H), 3.56 (br. s., 4H); $^{13}\text{C-NMR}$ (151 MHz, CDCl_3) δ 158.9, 155.0, 149.5, 136.8, 132.2, 129.5, 129.3, 128.8 (2), 126.6, 125.2 (2), 113.9, 107.7, 106.0, 99.1, 81.6, 80.4, 56.2, 52.4 (2), 50.9 (2), 50.7, 48.3 (d, $^1J_{\text{CF}} = 25.4$ Hz); HRMS calculated for $\text{C}_{25}\text{H}_{29}\text{FN}_5\text{O}_2$ (MH^+): 450.22998; Found: 450.22839.

1'-((5-methoxy-2-phenylbenzofuran-4-yl) methyl)-1,4'-bipiperidine (mBRef-1). Catalytic acetic acid (2 drops), followed by sodium cyanoborohydride (100 mg, 1.59 mmol, 2.0 eq) was added to a stirred solution of 5-methoxy-2-phenylbenzofuran-4-carbaldehyde (200 mg, 0.79 mmol, 1.0 eq) and 4-piperidinopiperidine (133 mg, 0.79 mmol, 1.0 eq) in methanol (20 mL). The mixture was stirred at room temperature for 48 h. The

solvent was removed under vacuum and the product was isolated by automated flash chromatography and RP-HPLC to yield mBRef-1 as a light yellow powder (187 mg, 58%); Mp: 225.3–229.0 °C; $^1\text{H-NMR}$ (500 MHz, CDCl_3) δ 7.88 (m, 2H), 7.45 (m, 2H), 7.36 (m, 2H), 7.27 (s, 1H), 6.90 (d, $J = 8.8$ Hz, 1H), 3.87 (s, 3H), 3.80 (s, 2H), 3.03 (d, $J = 11.7$ Hz, 2H), 2.50 (br. s., 4H), 2.22 (m, 1H), 2.07 (td, $J = 11.9$ Hz, $J = 2.0$ Hz, 2H), 1.78 (d, $J = 12.2$ Hz, 2H), 1.58 (br. s., 6H), 1.43 (br. s., 2H); $^{13}\text{C-NMR}$ (126 MHz, CDCl_3) δ 156.3, 154.0, 150.0, 130.9, 130.7, 128.7 (2), 128.4, 124.9 (2), 118.9, 109.7, 109.7, 101.6, 62.9, 57.4, 54.0, 53.6 (2), 50.3 (2), 28.2 (2), 26.4 (2), 24.8; HRMS calculated for $\text{C}_{26}\text{H}_{32}\text{N}_2\text{O}_2$ (MH^+): 405.25366; Found: 405.25227.

Radiochemistry

No-carrier-added (n.c.a.) [^{18}F]fluoride was produced via the ^{18}O (p, n) ^{18}F nuclear reaction by bombardment of an isotopically enriched [^{18}O]- H_2O target with either a 18 MeV or a 10 MeV proton beam generated by an IBA 18/9 or 10/5 cyclotron at the Austin Hospital (Heidelberg, Australia). [^{18}F]Fluoride was concentrated on a Waters Sep-Pak Accell Plus QMA Light cartridge which was conditioned with 10 mL 0.5 M aqueous potassium carbonate solution and washed with 10 mL water prior to use.

[^{18}F]1-((1-(2-Fluoroethyl)-1H-1,2,3-triazol-4-yl) methyl)-4-((5-methoxy-2-phenylbenzofuran-4-yl) methyl) piperazine ([^{18}F]mBPET-1). [^{18}F]Fluoride (3.7–74 GBq) was eluted from the QMA light ion exchange cartridge using a solution of 3.5 mg potassium carbonate in 200 μL water and 20 mg Kryptofix 2.2.2 in 400 μL acetonitrile. The eluate was dried azeotropically at 75 °C under vacuum and a gentle argon stream over 6 min followed by addition of 1 mL acetonitrile and drying at 120 °C under full vacuum for 5 min. 4.0 μL 2-azidoethyl-4-toluenesulfonate in 750 μL acetonitrile were added to the dry $^{18}\text{F}^-$ /cryptate and the reaction was heated to 90 °C for 7 min. [^{18}F]6 was distilled into a cooled vessel containing 3.0 mg alkyne-precursor 5. Subsequently a mixture of 6.0 mg tetrakis (acetonitrile) copper (I) hexafluorophosphate and 4.0 mg tris [(1-benzyl-1H-1,2,3-triazol-4-yl) methyl] amine (TBTA) in 300 μL DMF was added to the distilled product and heated to 70 °C for 30 min in a sealed reactor. The reaction was heated for another 7 min under vacuum before adding 1 mL acetonitrile and 4 mL water. The diluted mixture was purified on a semi-preparative RP-HPLC column (Phenomenex, Gemini 10u C18, 250 \times 10 mm, 10 μm ; gradient: 20–90% acetonitrile in 0.1 M aq. ammonium formate over 18 min; flow rate: 4 mL/min). [^{18}F]mBPET-1 eluted at 15 min and was diluted with 40 mL of deionized water upon collection, passed through a conditioned Phenomenex Strata-X C18 cartridge, washed with 10 mL of deionized water and reformulated using 2 mL DMSO. The overall radiochemical yield (RCY) of [^{18}F]mBPET-1 was 40% \pm 5% ($n = 6$) after 90 min. A sample of the reconstituted product was analysed by analytical RP-HPLC (Phenomenex, Gemini 5u C18, 150 \times 4.6 mm, 5 μm ; gradient: 5–90% acetonitrile in 0.1 M aq. ammonium formate over 18 min; flow rate: 0.5 mL/min, $t_{\text{R}} = 13.6$ min) to determine the molar activity and radiochemical purity.

Lipophilicity

The lipophilicity of [^{18}F]mBPET-1 was determined by addition of 444 kBq to a mixture of 800 μL *n*-octanol and 800 μL 0.1 M phosphate buffer (pH 7.4). The mixture was

vortexed for 3 min and centrifuged at 10,000 rpm for 5 min. The radioactivity in 100 μ L aliquots of each phase was measured in a gamma counter. Experiments were performed in triplicates.

Metabolic stability assay

The metabolic stability of [18 F]mBPET-1 was assessed using mouse S9 liver fractions. NADPH was generated in-situ using a NADPH generating system. To create 800 μ L of the NADPH generating stock 200 μ L aliquots of the following solutions were mixed: 9.3 mg glucose-6-phosphate in 250 μ L PBS; 9.95 mg β -nicotinamide adenine dinucleotide phosphate sodium salt hydrate (NADP sodium salt hydrate) in 250 μ L PBS; 6.7 mg magnesium chloride hexahydrate in 250 μ L Milli-Q water; 6 μ L (11.5 U) glucose-6-phosphate dehydrogenase (G-6-P-DH) stock solution in 1 mL PBS. The G-6-P-DH stock solution (2000 U/mL) was prepared by dissolving 2.33 mg protein in 1 mL PBS and stored at -30°C . The assay was carried out by mixing 230 μ L of PBS with 40 μ L NADPH generating solution, 15 μ L S9 liver fraction stock and 15 μ L analyte in 10% ethanol/saline containing about 3.7 MBq (100 μ Ci). The control study was prepared accordingly without the S9 liver fraction stock. The solutions were incubated at 37°C in a thermo shaker. Samples were quenched with 150 μ L methanol at various time points and centrifuged at 12,000 rpm for 10 min. The supernatant was analysed using radio-HPLC.

MTS proliferation assay

Two thousand five hundred cells per well were seeded in a 96-well plate with column 12 left as a blank and incubated in 50 μ L media overnight at 37°C . Subsequently, 50 μ L of media containing different concentrations of RAD001 was added to the wells. Drug media concentrations were prepared by performing 3:4 serial dilutions over 10 wells in triplicates on separate plates. The drug media was then transferred to the cell plates, leaving an “untreated” and a blank well. Cells were incubated for 3 days followed by addition of 20 μ L of MTS reagent. Plates were incubated for a further 90–180 min at 37°C before the absorption at 490 nm was measured on a microplate reader using a 650 nm reference. The average absorbance of the blank wells was subtracted from the absorbances in the untreated and treated wells. The latter were then expressed as percentiles of the average absorbance of untreated wells and normalized. EC50 values were determined using the PRISM software package and a four parameter variable slope non-linear curve fit. Experiments were performed in triplicates and repeated three times. Statistical significance was calculated using a one-way ANOVA comparison with Bonferroni post hoc test (**** indicates $p \leq 0.0001$).

Cell uptake assay

Four hundred thousand cells per well were seeded in a 6-well plate and incubated in 5 mL media overnight at 37°C . Subsequently the media was replaced with 2.0 mL media containing 1% FCS and wells were treated in triplicates with 370–555 kBq of [18 F]mBPET-1 in < 5% DMSO/media (0% FCS). For blocked experiments, cells were additionally treated with mBRef-1 at a concentration of 10 μ M. Plates were incubated as per their respective time points (5, 10, 15, 20, 30, 60, 90 and 120 min) and quenched

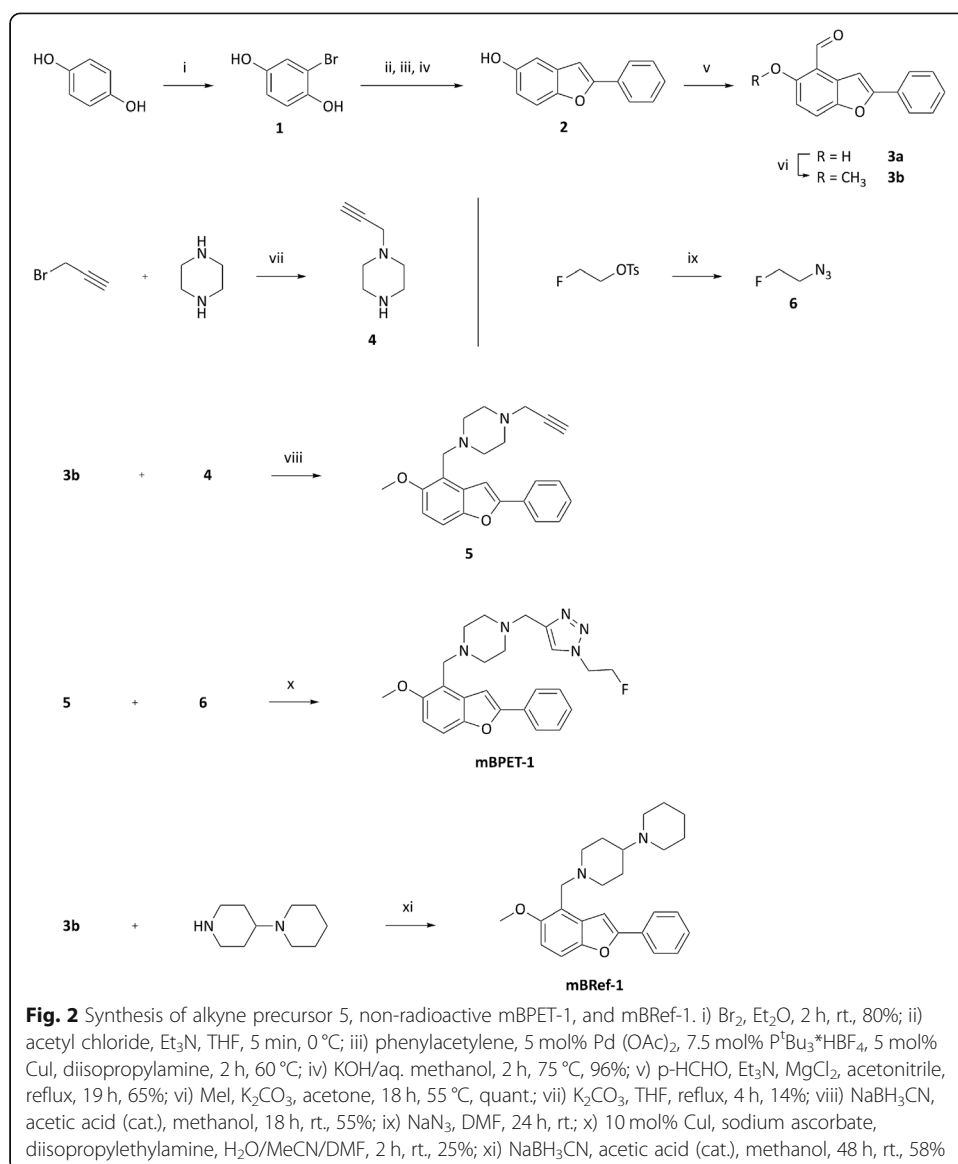
by removal of the media and washing twice with 0.5 mL cold PBS. The supernatant and washing solutions were combined and the radioactivity was measured in a gamma counter (S). Optionally, the second washing step was replaced by an acid wash to remove surface bound [^{18}F]mBPET-1 using 0.5 mL of cold 50 mM sodium acetate buffer (pH 5) followed by washing twice with 1 mL cold PBS. The acetate and PBS wash solutions were combined and the radioactivity was counted in a gamma counter (A). The cell pellet was lysed using 0.8 mL of cold 0.1 M sodium hydroxide solution and the lysate was collected. The well was rinsed twice with 1 mL cold PBS and the radioactivity in the combined fractions was determined in a gamma counter (P). Radioactivity readouts were correct for background radiation (*) and the cell uptake fraction of [^{18}F]mBPET-1 was calculated as: $P^* / (S^* + A^* + P^*)$. The cell surface bound fraction of [^{18}F]mBPET-1 was calculated as: $A^* / (S^* + A^* + P^*)$. Experiments were performed in triplicates and repeated 1–8 times. Statistical significance was calculated using a non-parametric one-way ANOVA comparison with Dunn's post hoc testing (* indicates $p \leq 0.05$, ** indicates $p \leq 0.01$, *** indicates $p \leq 0.001$, **** indicates $p \leq 0.0001$).

Results and discussion

Initially, the synthesis towards mBPET-1 was based closely on results from the structural optimisation work described above. The published reaction sequence relies on a Mannich reaction which could not be reproduced with the building blocks used in this work. Replacement with a sequence of ortho-formylation and subsequent reductive amination allowed access to different amino methylated compounds in reproducible yields (Fig. 2).

In the first step, hydroquinone was brominated using bromine to give the monobrominated product 1 in 80% yield. Bromination in more than one position was not observed. Bromohydroquinone was then reacted with acetyl chloride to mask the hydroxyl groups as acetoxy groups. The protected compound and phenylacetylene were then subjected to Sonogashira conditions using copper iodide and palladium / tri-*tert*-butylphosphine catalyst systems and diisopropylamine as a base. The initial protection step, the cross-coupling reaction as well as the subsequent deprotection and condensation with potassium hydroxide were carried out in a one-pot fashion without intermediate purification. Chromatographic isolation gave the fully formed benzofuran 2 in excellent yields up to 96%. Ring closure was confirmed using DEPT135 and standard ^{13}C -NMR spectroscopy. Over the course of the furan ring formation, the number of quaternary carbons in the compound is reduced from 6 to 5 which was confirmed in the recorded spectra. Scale-up did not affect the Sonogashira reaction negatively and yields were consistently high when the reaction mixture was carefully degassed prior to heating the reaction (Elangovan et al. 2003). Oxygen contamination is known to lead to homocoupling between terminal alkynes as described by the Glaser coupling (Glaser 1869; Glaser 1870). The corresponding product, 1,3-butadiyne, was detected in reaction mixtures that showed reduced yields.

A two-step procedure to *ortho*-formylate benzofuran substrates using ethyl *N*-phenylformimidate to form the imine followed by hydrolysis under acidic conditions has been reported (Andrew et al. 1999). A more convenient method published by Hofsløkken and Skattebøl describes the *ortho*-formylation of various phenols in one step (Hofsløkken and Skattebøl 1999). The scope of this reaction, now called Casnati-Skattebøl



formylation, has recently been expanded (Akselsen et al. 2009; Hansen and Skattebøl 2005; Hansen and Skattebol 2012; Pergomet et al. 2017). Although this method had not been tested on benzofurans, it was investigated whether 2 could be formylated using the reported conditions. The reaction requires a minimum of 2 equivalents of formaldehyde relative to the amount of phenol. Using 6 equivalents, formation of the aldehyde in one step was achieved in 65% yield. Magnesium chloride which acts as a Lewis acid coordinates to the phenol and formaldehyde, directing it into the least sterically hindered *ortho*-position. Neither the 4- nor the 6-position of 2 are particularly crowded hence regioselectivity was expected to be poor. However, the reaction gave 3a as the major product as confirmed by the presence of vicinal proton coupling in the ¹H-NMR spectrum between the protons in 6- and 7-position (Additional file 1: Figure S3 a/c).

Preparation of 1-(Prop-2-yn-1-yl) piperazine (4) was attempted at low temperatures following published procedures (Castelhana et al. 2003; Hamann et al. 2014; Kushwaha and Kaushik 2014). However, product could only be isolated when the reaction was

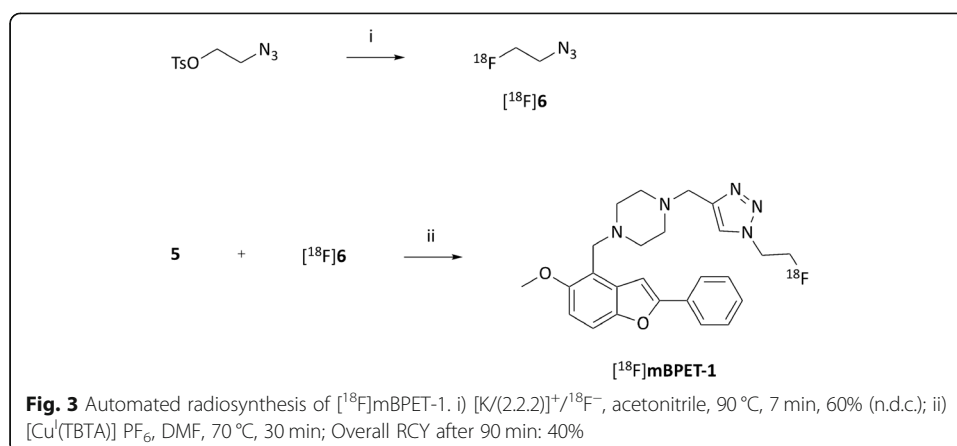
performed at elevated temperatures in THF using potassium carbonate as a base. Alkylation of piperazine with propargyl bromide under these conditions gave 4 in 14% isolated yield. Methylation of the hydroxyl group on 3a and reductive amination of the carbonyl with 4 using sodium cyanoborohydride and catalytic amounts of acetic acid in methanol gave the alkyne 5 in 55% yield (Abdel-Magid and Mehrman 2006). mBRef-1 was prepared following the same procedure used to produce 5 and resulted in a comparable yield of 58%. Compounds 5 and mBRef-1 were purified by semi-preparative RP-HPLC before being employed in Click reactions or as a blocking agent, respectively.

2-Fluoroethylazide (6) was synthesised following a previously published procedure (Ackermann et al. 2011; Glaser and Årstad 2007). Briefly, 2-fluoroethyl 4-toluenesulfonate was treated with sodium azide at room temperature for 24 h. The crude reaction mixture was used in the next step without prior purification. A copper (I) source in conjunction with 10 mol% of a reducing agent was used as a catalyst for the 1,3-dipolar cycloaddition between 5 and 6 which gave the 1,4-substituted triazole mBPET-1 in 25% yield (Hein and Fokin 2010; Meldal and Tornøe 2008). ¹H-NMR analysis of mBPET-1 showed a singlet at 7.90 ppm corresponding to the 1,2,3-triazole proton and the characteristic fluorine splitting of the protons on the fluoroethyl group (Additional file 1: Figure S7 a). MS analysis showed a signal at $m/z = 450.22839$ which correlates to the MH^+ signal of mBPET-1 with a mass error of -3.5 ppm (Additional file 1: Figure S7 c).

Radiosynthesis of [¹⁸F]mBPET-1 was achieved using copper catalysed click chemistry similarly to the synthesis of the non-radioactive derivative mBPET-1 (Fig. 3). 2-Azidoethyl-4-toluenesulfonate was treated with activated n.c.a. [¹⁸F] fluoride to give 2-[¹⁸F]fluoroethylazide ([¹⁸F]6) which was purified by distillation. Cycloaddition of [¹⁸F]6 to 5 was carried out using a Cu (I)/TBTA catalyst system. All steps were performed using the iPHASE Flexlab (Melbourne, Australia) automated synthesis module (Fig. 4). The previously published procedure was modified to facilitate radiosynthesis of [¹⁸F]mBPET-1 (Ackermann et al. 2014).

Briefly, aqueous [¹⁸F]fluoride from the cyclotron target was concentrated on an ion exchange cartridge, eluted into reactor 1 (Fig. 4 - R1) with a solution of K₂CO₃/Kryptofix and dried azeotropically. The dry [¹⁸F]F⁻/cryptate was heated with 2-azidoethyl-4-toluenesulfonate and the product was subsequently isolated via distillation by heating / pressurising reactor 1 and cooling / evacuating reactor 2 (Fig. 4 - R2). Residual [¹⁸F]6 remaining in the tubing after the distillation was recovered by transferring a small volume of DMF from vial 7 into reactor 2. The distillate was then reacted with precursor 5 using a Cu (I)/TBTA catalyst. After evaporation of unreacted [¹⁸F]6 the resulting mixture was diluted with acetonitrile and water. [¹⁸F]mBPET-1 was isolated using HPLC-column B and collected in HPLC flask 2. The diluted product was concentrated on a C18 cartridge, washed with water and reformulated in DMSO.

Nucleophilic substitution typically afforded [¹⁸F]6 in 60% n.d.c. yield after distillation. The distillation process can be monitored via the radioactivity traces of R1 and R2 and should follow the trend shown in Fig. 5a. The crude triazole [¹⁸F]mBPET-1 was purified using semi-preparative RP-HPLC followed by reformulation using a polymer-based C18 cartridge. The overall radiochemical yield was $40\% \pm 5\%$ ($n = 6$) after 90 min of synthesis. The radiochemical purity was always $\geq 99\%$ at end of synthesis (EOS) and $\geq 98\%$



after 4 h at room temperature in DMSO (Additional file 1: Table S2). The typical molar activity was 24.8 GBq/ μmol (EOS) with a maximum of 78.6 GBq/ μmol (EOS) produced. The logarithmic *n*-octanol/water distribution coefficient at pH 7.4 ($\log D_{7.4}$) was determined to be 0.89 (Additional file 1: Table S1). [^{18}F]mBPET-1 showed high metabolic stability. Incubation with mouse S9 liver fractions at 37 °C resulted in a 0.8% drop in radiochemical purity after 3 h compared to a control (Additional file 1: Table S3). Coinjection of [^{18}F]mBPET-1 and mBPET-1 confirmed the identity of the radiolabelled material (Fig. 6).

To investigate the ability of [^{18}F]mBPET-1 to distinguish between RAD001 sensitive and insensitive tumour populations, breast cancer cell lines with high and low sensitivity to RAD001 were selected (Hurvitz et al. 2015b). HCC-1419 is a luminal breast cancer cell line with positive HER2 and estrogen receptor (ER) status. The reported average half maximal inhibitory concentration (IC₅₀) when treated with RAD001 is 0.20 nM and average inhibition at 100 nM is > 100%, which classifies this cell line as RAD001 sensitive according to Hurvitz et al.. MDA-MB-468 is a basal breast cancer

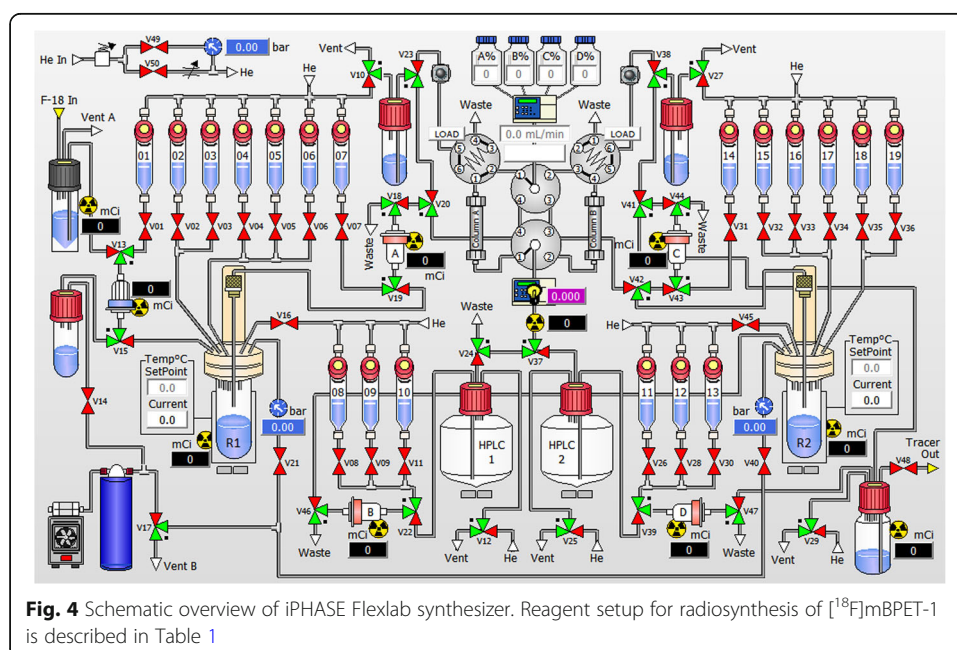
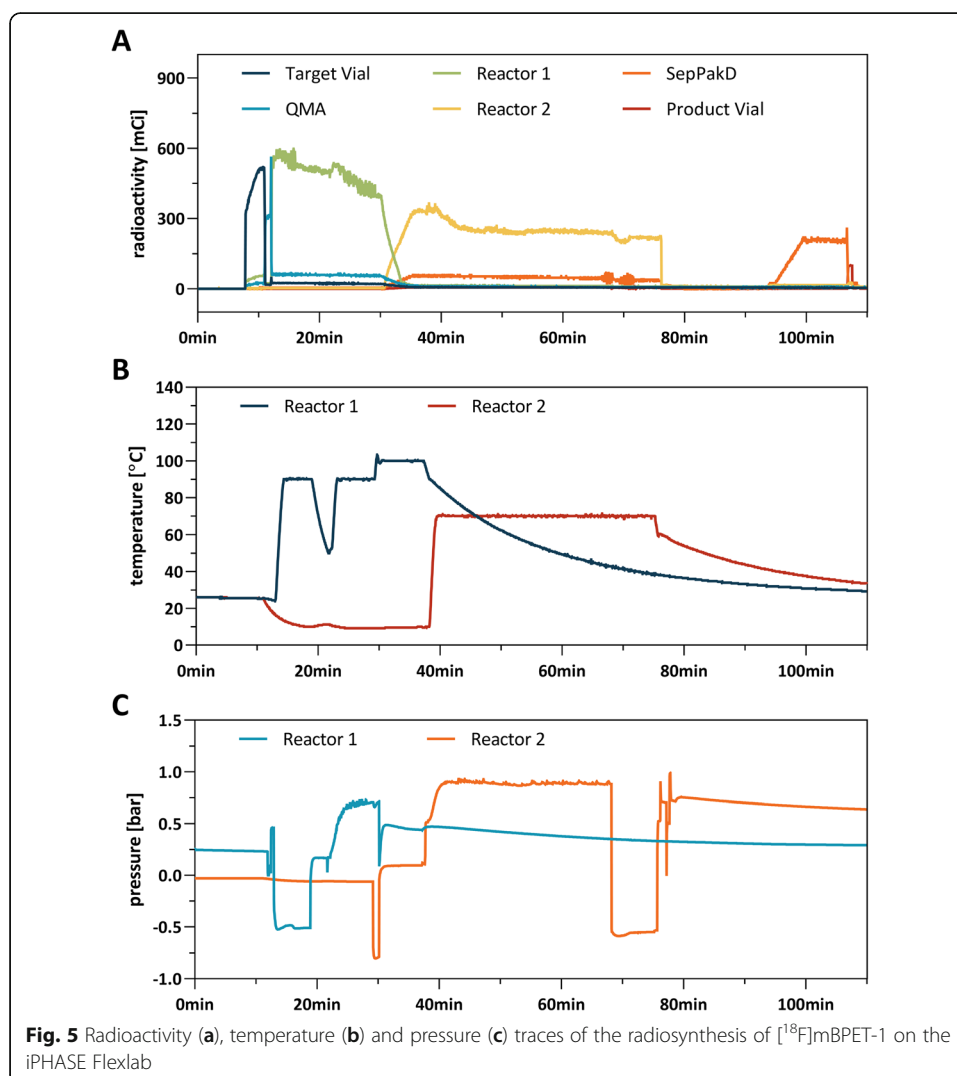
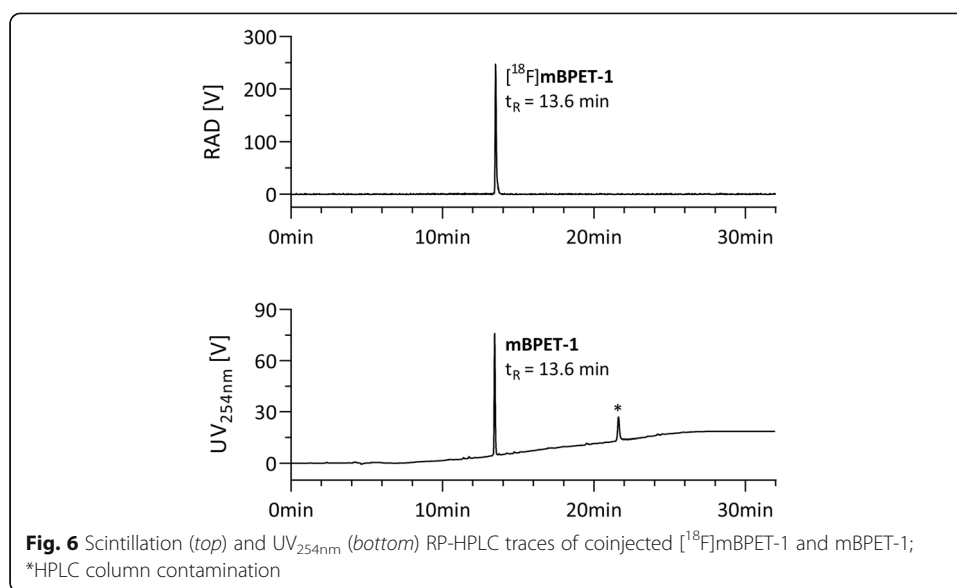


Table 1 Reagent setup to enable automated radiosynthesis of [^{18}F]mBPET-1 on iPHASE Flexlab

location	reagent
QMA	Waters QMA Light (activated with 10 mL 0.5 M K_2CO_3)
Sep-Pak D	Phenomenex Strata-X C18 (conditioned with EtOH/ H_2O)
vial 1	3.5 mg K_2CO_3 in 200 μL H_2O + 20.0 mg K_{222} in 400 μL MeCN
vial 2	4.0 μL 2-azidoethyl-4-toluenesulfonate in 750 μL MeCN
vial 3	1.0 mL MeCN
vial 7	100 μL DMF
vial 11	10 mL H_2O
vial 12	1.0 mL DMSO
vial 13	1.0 mL DMSO
vial 17	4 mL H_2O
vial 18	1.0 mL MeCN
vial 19	6.0 mg $\text{Cu}(\text{CH}_3\text{CN})_4\text{PF}_6$ + 4.0 mg TBTA in 300 μL DMF
HPLC-2 flask	40 mL H_2O
reactor 2	3.0 mg precursor 5 (neat)

**Fig. 5** Radioactivity (a), temperature (b) and pressure (c) traces of the radiosynthesis of [^{18}F]mBPET-1 on the iPHASE Flexlab

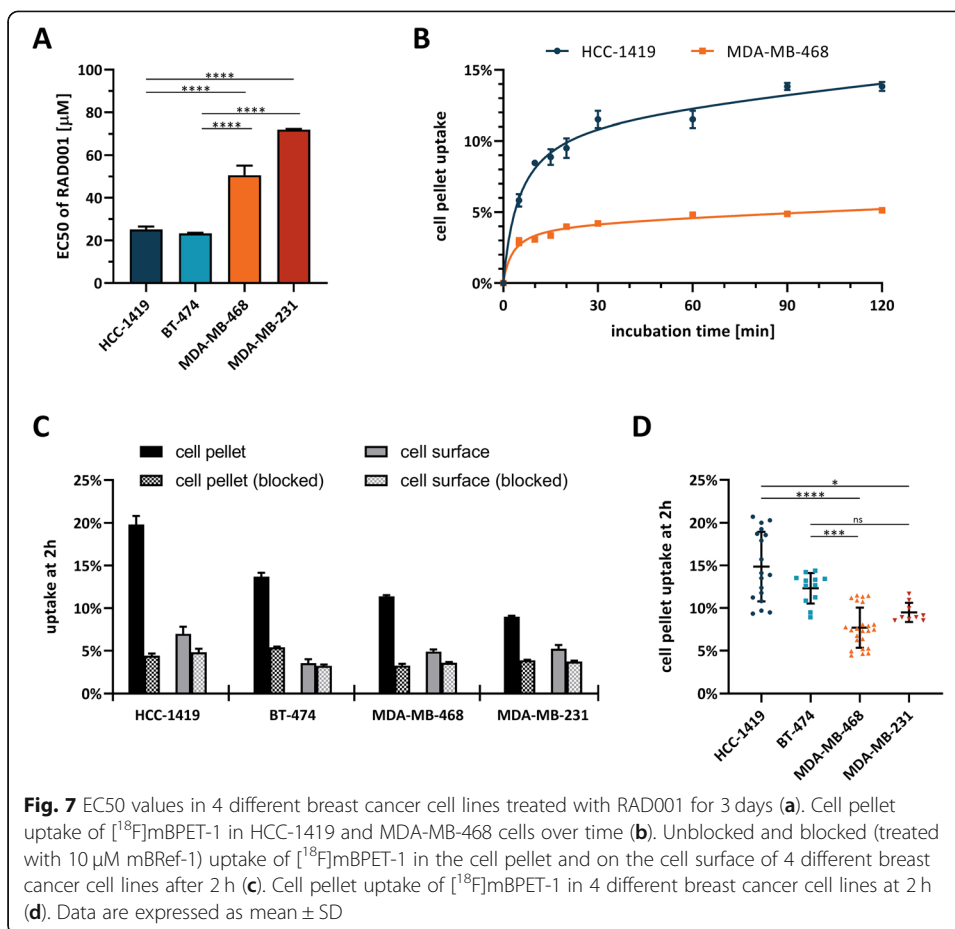


cell line with normal HER2 and negative ER status. The reported IC₅₀ value when treated with RAD001 is > 100 nM with an average inhibition of 48.9% at that concentration. MDA-MB-468 is classified as a RAD001 resistant cell line, although the term insensitive would be more suitable due to the fact that these cells still show some response to RAD001 treatment.

The reported RAD001 sensitivity of these cell lines was confirmed by determining the half maximal effective concentration (EC₅₀) using the colorimetric MTS proliferation assay (Additional file 1: Table S4). Cytotoxicity of RAD001 was significantly different to the vehicle control in all cell lines at higher concentrations (Additional file 1: Figure S9). Mean EC₅₀ values of RAD001 in HCC-1419 and BT-474 cells were 25.17 μM ± 1.14 μM and 23.27 μM ± 0.29 μM, respectively (Fig. 7a). Mean EC₅₀ values of RAD001 in MDA-MB-468 and MDA-MB-231 cells were 50.65 μM ± 3.64 μM and 72.02 μM ± 0.26 μM, respectively. While the absolute EC₅₀ values differ from the reported IC₅₀ data, presumably due to the different assay used by Hurvitz et al., the overall trend of high/low RAD001 sensitivity was confirmed. Based on these results, the HCC-1419/BT-474 and MDA-MB-468/MDA-MB-231 cell lines were used as a model system for RAD001 treatment sensitivity.

Initially, dynamic cell uptake of [¹⁸F]mBPET-1 was investigated in vitro in HCC-1419 and MDA-MB-468 cell lines over a time frame of 120 min (Fig. 7b). Uptake in the cell pellet was used as an indicator of mTOR expression or activation levels and should correlate with the RAD001 sensitivity of each cell line. The kinetic profiles of [¹⁸F]mBPET-1 were similar in both cell lines reaching an uptake equilibrium after incubation for 60–90 min at 37 °C. Uptake of [¹⁸F]mBPET-1 in RAD001 sensitive HCC-1419 cells reached 13.8% ± 0.2% at equilibrium compared to 4.9% ± 0.1% in RAD001 insensitive MDA-MB-468 cells (Additional file 1: Table S5). The maximum ratio of the cell pellet uptake between the two cell lines was 2.83.

Uptake specificity was determined by treating cells with mBRef-1 at a concentration of 10 μM, in addition to [¹⁸F]mBPET-1 (Fig. 7c). mBRef-1 competes with [¹⁸F]mBPET-



1 for the same binding sites and thereby reduces target specific binding of the latter. mBRef-1 competition reduced uptake of [¹⁸F]mBPET-1 in all cell lines indicating that there is target specific binding in each of them. This is not surprising considering mTOR is central to survival and a natural component of cells. Interestingly, the level of [¹⁸F]mBPET-1 uptake in blocked experiments seems to be similar across cell lines (Additional file 1: Table S6). This indicates a general pool of non-specific uptake. In this experiment, cell surface bound [¹⁸F]mBPET-1 was removed by including an acidic washing step with 50 mM acetate buffer pH 5. Blocking showed that while there is considerable binding to the cell surface (3.6% - 7.0%), this is mostly non-specific (specific binding: 0.3% - 2.2%).

Figure 7d shows a summary of [¹⁸F]mBPET-1 cell uptake after incubation for 2 h from multiple experiments performed in triplicate (Additional file 1: Table S7). Mean uptake in RAD001 sensitive HCC-1419 and BT-474 cell lines is $14.9\% \pm 4.0\%$ ($n = 6$) and $12.3\% \pm 1.7\%$ ($n = 4$), respectively. Mean uptake in RAD001 insensitive MDA-MB-468 and MDA-MB-231 cell lines is $7.7\% \pm 2.3\%$ ($n = 8$) and $9.5\% \pm 1.1\%$ ($n = 3$), respectively. The difference in [¹⁸F]mBPET-1 uptake between either of the RAD001 sensitive cell lines and MDA-MB-468 is highly significant. A weaker, but statistically significant difference between HCC-1419 and MDA-MB-231 cells is also evident.

While these preliminary experiments suggest that [¹⁸F]mBPET-1 may be a suitable probe to distinguish between RAD001 sensitive and insensitive cell lines, more work is

required to characterise the relation between mTOR expression / activation and RAD001 sensitivity in the employed cell lines.

Conclusion

In conclusion, we synthesized a substituted benzofuran scaffold equipped with an alkyne in 27.5% yield over 7 linear steps. Fully automated radiolabelling using Click chemistry proceeded in 40% RCY and gave [^{18}F]mBPET-1 in excellent radiochemical purity and good molar activity. In vitro studies confirmed the specificity of observed cell uptake and showed 1.3–1.9-fold increased cell uptake of [^{18}F]mBPET-1 in RAD001 sensitive compared to RAD001 insensitive cells across 4 breast cancer cell lines. These results warrant further studies in murine xenografts to expand on the biological properties of this molecular probe and evaluate its suitability as a predictor of RAD001 treatment response.

Supplementary information

Supplementary information accompanies this paper at <https://doi.org/10.1186/s41181-020-0089-9>.

Additional file 1: Figure S1a. $^1\text{H-NMR}$ of 2-Bromo-1,4-dihydroxybenzene. **Figure S2a.** $^1\text{H-NMR}$ of 2-Phenylbenzofuran-5-ol. **Figure S3a.** $^1\text{H-NMR}$ of 5-hydroxy-2-phenylbenzofuran-4-carbaldehyde (**3a**). **Figure S4a.** $^1\text{H-NMR}$ of 5-Methoxy-2-phenylbenzofuran-4-carbaldehyde (**3b**). **Figure S5a.** $^1\text{H-NMR}$ of 1-(Prop-2-yn-1-yl) piperazine. **Figure S6a.** $^1\text{H-NMR}$ of 1-((5-Methoxy-2-phenylbenzofuran-4-yl) methyl)-4-(prop-2-yn-1-yl) piperazine (**5**). **Figure S7a.** $^1\text{H-NMR}$ of 1-((1-(2-Fluoroethyl)-1H-1,2,3-triazol-4-yl) methyl)-4-((5-methoxy-2-phenylbenzofuran-4-yl) methyl) piperazine (**mBPET-1**). **Figure S8a.** $^1\text{H-NMR}$ of 1'-((5-methoxy-2-phenylbenzofuran-4-yl) methyl)-1,4'-bipiperidine (**mBRef-1**). **Table S1.** Distribution coefficient of [^{18}F]mBPET-1 @ pH 7.4. **Table S2.** Radiochemical purity of [^{18}F]mBPET-1 incubated in DMSO at room temperature. **Table S3.** Radiochemical purity (RP) of [^{18}F]mBPET-1 incubated with or without (control) mouse S9 liver fractions at 37 °C as determined by RP-HPLC. **Table S4a.** MTS cytotoxicity assays of HCC-1419 breast cancer cells treated with either RAD001 or vehicle control (DMSO) for 3 days. **Figure S9.** Summary of MTS cytotoxicity assays in 4 different breast cancer cell lines. Experiments were performed in triplicates and repeated three times. Data are expressed as their mean \pm SD. **Table S5.** Cell uptake assay of [^{18}F]mBPET-1 in HCC-1419 and MDA-MB-468 breast cancer cells from 0 to 120 min. Cell uptake expressed as the percentile of decay corrected total dose added to cells. **Table S6a.** Blocked and unblocked cell pellet uptake of [^{18}F]mBPET-1 after incubation for 2 h at 37 °C. **Table S7.** Cell pellet uptake of [^{18}F]mBPET-1 after incubation for 2 h at 37 °C. Summary of multiple experiments performed in triplicates.

Abbreviations

AKT: Protein kinase B; CDK4/6: Cyclin-dependent kinase 4/6; DEPT: Distortionless enhancement by polarization transfer; DMF: Dimethylformamide; DMSO: Dimethyl sulfoxide; EC50: Half maximal effective concentration; EOS: End of synthesis; ER+/-: Estrogen receptor positive/negative; ESI-MS: Electrospray ionization mass spectrometry; FT-ICR: Fourier-transform ion cyclotron resonance; G-6-P-DH: Glucose-6-phosphate dehydrogenase; HER2: Human epidermal growth factor receptor 2; HR+/-: Hormone receptor positive/negative; HRMS: High resolution mass spectrometry; HTS: High throughput screening; IC50: Half maximal inhibitory concentration; IHC: Immunohistochemistry; LCMS: Liquid chromatography coupled to mass spectrometry; m/z: MASS (m) to charge (z) ratio; mBPET-1: mTOR Benzofuran PET compound - derivative 1; mBRef-1: mTOR Benzofuran Reference compound - derivative 1; MeV: Megaelectronvolt; Mp: Melting point; mTOR: mammalian target of rapamycin; mTORC1: mTOR complex 1; MTS: 3-(4,5-Dimethylthiazol-2-yl)-5-(3-carboxymethoxyphenyl)-2-(4-sulfophenyl)-2H-tetrazolium; n.c.a.: no-carrier-added; n.d.c.: non decay-corrected; NADPH/NADP: Nicotinamide adenine dinucleotide phosphate; NMR: Nuclear magnetic resonance; P: Cell pellet fraction; PBS: Phosphate buffered saline; PDK1: Phosphoinositide-dependent kinase-1; PET: Positron emission tomography; PI3K: Phosphatidylinositol 3-kinase; pS6: phospho-S6; PTEN: Phosphatase and tensin homolog; RAD001: Everolimus; RCY: Radiochemical yield (as defined by SRS); RP-HPLC: Reversed-phase high-performance liquid chromatography; S: Supernatant fraction; SD: Standard deviation; SPE: Solid phase extraction; SPECT: Single-photon emission computed tomography; TBTA: Tris [(1-benzyl-1H-1,2,3-triazol-4-yl) methyl] amine; THF: Tetrahydrofuran; TLC: Thin layer chromatography; TOF: Time of flight; U: Enzyme unit; UHPLC: Ultra-high performance liquid chromatography

Acknowledgements

The authors would like to thank the Department of Molecular Imaging and Therapy at Austin Health for providing access to their facilities including the use of their cyclotron and automated synthesis modules, the Mass Spectrometry and Proteomics Facility (MSPF) at the Bio21 Institute - The University of Melbourne for providing access to HRMS and HPLC systems, and the Olivia Newton-John Cancer Research Institute (ONJCRI) for providing access to their PC2 laboratories.

Authors' contributions

CWW conceived the design of the ligand and its synthetic pathway and performed non-radioactive syntheses, fluorine-18 labelling, metabolic stability studies, cell culture and radioactive cell uptake assays. YWG developed the fluorine-18 labelling protocol and assisted with the automation of the procedure. NG performed cell culture and MTS assays. ACP enabled and provided guidance on in vitro studies and assisted with cell culture. AR assisted with the design and execution of the radioactive cell uptake assays. JMW provided guidance and oversight over non-radioactive syntheses. UA provided guidance and oversight over radiolabelling experiments and assisted with ligand design. AMS provided guidance and oversight over in vitro experiments. CWW wrote the manuscript under guidance from AMS, UA and JMW. All authors read and approved the final manuscript.

Funding

This work was funded by NHMRC grants 1092788 and 1084178. Further partial support was provided by a La Trobe University Understanding Disease Research Focus Area – Mini Start-Up Project grant.

Availability of data and materials

The datasets used and/or analysed during the current study are available from the corresponding author on reasonable request.

Ethics approval and consent to participate

Not applicable.

Consent for publication

Not applicable.

Competing interests

The authors declare that they have no competing interests.

Author details

¹The University of Melbourne, Parkville, VIC 3010, Australia. ²Department of Molecular Imaging and Therapy, Austin Hospital, 145 Studley Road, Heidelberg, VIC 3084, Australia. ³Olivia Newton-John Cancer Research Institute, 145 Studley Road, Heidelberg, VIC 3084, Australia. ⁴School of Cancer Medicine, La Trobe University, Plenty Road & Kingsbury Drive, Bundoora, VIC 3086, Australia.

Received: 28 October 2019 Accepted: 6 January 2020

Published online: 23 January 2020

References

- Abdel-Magid AF, Mehrman SJ. A review on the use of sodium Triacetoxyborohydride in the reductive amination of ketones and aldehydes. *Org Process Res Dev.* 2006;10(5):971–1031.
- Ackermann U, O'Keefe G, Lee ST, Rigopoulos A, Cartwright G, Sachinidis JJ, et al. Synthesis of a [18F] fluoroethyltriazolylthymidine radiotracer from [18F]2-fluoroethyl azide and 5-ethynyl-2'-deoxyuridine. *J Label Compd Radiopharm.* 2011;54(5):260–6.
- Ackermann U, Plougastel L, Goh YW, Yeoh SD, Scott AM. Improved synthesis of [18F] FLETT via a fully automated vacuum distillation method for [18F]2-fluoroethyl azide purification. *Appl Radiat Isot.* 2014;94:72–6.
- Adams HJA, Kwee TC, de Keizer B, Fijnheer R, de Klerk JMH, Nievelstein RAJ. FDG PET/CT for the detection of bone marrow involvement in diffuse large B-cell lymphoma: systematic review and meta-analysis. *Eur J Nucl Med Mol Imaging.* 2014; 41(3):565–74.
- Akita T. Reaction of organic compounds with hydrazine. XI. Reaction of Quinone compounds with hydrazine hydrate. *Yakugaku Zasshi.* 1962;82(1):91–5.
- Akselsen ØW, Skattebøl L, Hansen TV. Ortho-formylation of oxygenated phenols. *Tetrahedron Lett.* 2009;50(46):6339–41.
- Altine B, Gai Y, Han N, Jiang Y, Ji H, Fang H, et al. Preclinical evaluation of a Fluorine-18 (18F)-labeled phosphatidylinositol 3-kinase inhibitor for breast cancer imaging. *Mol Pharm.* 2019;16(11):4563–71.
- Alvey L, Prado S, Huteau V, Saint-Joanis B, Michel S, Koch M, et al. A new synthetic access to furo [3,2-f] chromene analogues of an antimycobacterial. *Bioorg Med Chem.* 2008;16(17):8264–72.
- Andre F, Campone M, O'Regan R, Manlius C, Massacesi C, Tarek S, et al. Phase I study of Everolimus plus weekly paclitaxel and Trastuzumab in patients with metastatic breast cancer pretreated with Trastuzumab. *J Clin Oncol.* 2010;28(34):5110–5.
- Andre F, O'Regan R, Ozguroglu M, Toi M, Xu B, Jerusalem G, et al. Everolimus for women with trastuzumab-resistant, HER2-positive, advanced breast cancer (BOLERO-3): a randomised, double-blind, placebo-controlled phase 3 trial. *Lancet Oncol.* 2014;15(6):580–91.
- Andrew M, Birch AM, Bradley PA. A convenient synthetic route to 7,8-fused heterocyclic ring derivatives of (S)-2,3-Dihydro-1,4-benzodioxin-2-methanol. *Synthesis.* 1999;1999(07):1181–7.
- Bardia A, Hurvitz SA, DeMichele A, Clark AS, Zelnak AB, Yardley DA, et al. Triplet therapy (continuous ribociclib, everolimus, exemestane) in HR+/HER2– advanced breast cancer postprogression on a CDK4/6 inhibitor (TRINITY-1): efficacy, safety, and biomarker results. *J Clin Oncol.* 2019;37(15_suppl):1016.
- Baselga J, Campone M, Piccart M, Burris HA, Rugo HS, Sahnoud T, et al. Everolimus in postmenopausal hormone-receptor-positive advanced breast cancer. *N Engl J Med.* 2011;366(6):520–9.
- Baselga J, Tripathy D, Mendelsohn J, Baughman S, Benz CC, Dantis L, et al. Phase II study of weekly intravenous recombinant humanized anti-p185HER2 monoclonal antibody in patients with HER2/neu-overexpressing metastatic breast cancer. *J Clin Oncol.* 1996;14(3):737–44.
- Bjornsti M-A, Houghton PJ. The TOR pathway: a target for cancer therapy. *Nat Rev Cancer.* 2004;4:335.

- Castelhana A, McKibben B, Steinig A. Inventors; Google patents, assignee. Sedative, vasodilation, antiarrhythmia agents, antiallergens, antiinflammatory agents patent US20030229067 A1; 2003.
- Cobleigh MA, Vogel CL, Tripathy D, Robert NJ, Scholl S, Fehrenbacher L, et al. Multinational study of the efficacy and safety of humanized anti-HER2 monoclonal antibody in women who have HER2-overexpressing metastatic breast cancer that has progressed after chemotherapy for metastatic disease. *J Clin Oncol.* 1999;17(9):2639.
- Elangovan A, Wang Y-H, Ho T-I. Sonogashira coupling reaction with diminished Homocoupling. *Org Lett.* 2003;5(11):1841–4.
- Fei B, Schuster DM. PET molecular imaging-directed biopsy: a review. *AJR Am J Roentgenol.* 2017;209(2):255–69.
- Gajria D, Chandralapaty S. HER2-amplified breast cancer: mechanisms of trastuzumab resistance and novel targeted therapies. *Expert Rev Anticancer Ther.* 2011;11(2):263–75.
- Gayle SS, Arnold SLM, O'Regan RM, Nahta R. Pharmacologic inhibition of mTOR improves Lapatinib sensitivity in HER2-overexpressing breast cancer cells with primary Trastuzumab resistance. *Anti Cancer Agents Med Chem.* 2012;12(2):151–62.
- Glaser C. Beiträge zur Kenntniss des Acetylnylbenzols. *Ber Dtsch Chem Ges.* 1869;2(1):422–4.
- Glaser C. Untersuchungen über einige derivate der Zimmtsäure. *Justus Liebigs Annalen der Chemie.* 1870;154(2):137–71.
- Glaser M, Årstad E. "Click labeling" with 2-[18F] Fluoroethylazide for positron emission tomography. *Bioconjug Chem.* 2007;18(3):989–93.
- Gnant M. The role of mammalian target of rapamycin (mTOR) inhibition in the treatment of advanced breast cancer. *Curr Oncol Rep.* 2013;15(1):14–23.
- Grinev AN, Bon-Khvar P, Terent'ev AP. Quinones. XV. Condensation of p-benzoquinone with benzoylacetate ester. *Russ J Gen Chem.* 1957;27(0):821–3.
- Hamann AR, de Kock C, Smith PJ, van Otterloo WAL, Blackie MAL. Synthesis of novel triazole-linked mefloquine derivatives: biological evaluation against plasmodium falciparum. *Bioorg Med Chem Lett.* 2014;24(23):5466–9.
- Han N, Jiang Y, Gai Y, Liu Q, Yuan L, Wang Y, et al. (11) C-labeled Pictilisib (GDC-0941) as a molecular tracer targeting phosphatidylinositol 3-kinase (PI3K) for breast cancer imaging. *Contrast Media Mol Imaging.* 2019;2019:1760184.
- Hansen TV, Skattebøl L. Ortho-formylation of phenols; preparation of 3-Bromosalicylaldehyde. *Org Synth.* 2005;82:64–8.
- Hansen TV, Skattebøl L. Discussion addendum for: ortho-formylations of phenols; preparation of 3-Bromosalicylaldehyde. *Org Synth.* 2012;89:220–9.
- Hein JE, Fokin VV. Copper-catalyzed azide-alkyne cycloaddition (CuAAC) and beyond: new reactivity of copper (I) acetylides. *Chem Soc Rev.* 2010;39(4):1302–15.
- Hofsløkken NU, Skattebøl L. Convenient method for the ortho-formylation of phenols. *Acta Chem Scand.* 1999;53:258–62.
- Hurvitz SA, Andre F, Jiang Z, Shao Z, Mano MS, Neciosup SP, et al. Combination of everolimus with trastuzumab plus paclitaxel as first-line treatment for patients with HER2-positive advanced breast cancer (BOLERO-1): a phase 3, randomised, double-blind, multicentre trial. *Lancet Oncol.* 2015a;16(7):816–29.
- Hurvitz SA, Dalenc F, Campane M, O'Regan RM, Tjan-Heijnen VC, Gligorov J, et al. A phase 2 study of everolimus combined with trastuzumab and paclitaxel in patients with HER2-overexpressing advanced breast cancer that progressed during prior trastuzumab and taxane therapy. *Breast Cancer Res Treat.* 2013;141(3):437–46.
- Hurvitz SA, Kalous O, Conklin D, Desai AJ, Dering J, Anderson L, et al. In vitro activity of the mTOR inhibitor everolimus, in a large panel of breast cancer cell lines and analysis for predictors of response. *Breast Cancer Res Treat.* 2015b;149(3):669–80.
- Jerusalem G, Fasolo A, Dieras V, Cardoso F, Bergh J, Vittori L, et al. Phase I trial of oral mTOR inhibitor everolimus in combination with trastuzumab and vinorelbine in pre-treated patients with HER2-overexpressing metastatic breast cancer. *Breast Cancer Res Treat.* 2011;125(2):447–55.
- Kau TR, Schroeder F, Ramaswamy S, Wojciechowski CL, Zhao JJ, Roberts TM, et al. A chemical genetic screen identifies inhibitors of regulated nuclear export of a Forkhead transcription factor in PTEN-deficient tumor cells. *Cancer Cell.* 2003;4(6):463–76.
- Krug B, Crott R, Lonnew M, Baurain J-F, Pirson A-S, Vander BT. Role of PET in the initial staging of cutaneous malignant melanoma: systematic review. *Radiology.* 2008;249(3):836–44.
- Kushwaha K, Kaushik N, Lata, Jain SC. Design and synthesis of novel 2H-chromen-2-one derivatives bearing 1,2,3-triazole moiety as lead antimicrobials. *Bioorg Med Chem Lett.* 2014;24(7):1795–801.
- Laes J-F, Sauvage S, Ghitti G. Tumor-biopsy stratification based on mTOR-pathway activity and functional mutations in the upstream genes PIK3CA and PTEN. *Oncotarget.* 2017;8(48):84426–33.
- Lau DK, Tay RY, Yeung YH, Chionh F, Mooi J, Murone C, et al. Phase II study of everolimus (RAD001) monotherapy as first-line treatment in advanced biliary tract cancer with biomarker exploration: the RADiChol study. *Br J Cancer.* 2018;118(7):966–71.
- Liu Q, Xu C, Kirubakaran S, Zhang X, Hur W, Liu Y, et al. Characterization of Torin2, an ATP-competitive inhibitor of mTOR, ATM, and ATR. *Cancer Res.* 2013;73(8):2574–86.
- Lu C-H, Wyzomierski SL, Tseng L-M, Sun M-H, Lan K-H, Neal CL, et al. Preclinical testing of clinically applicable strategies for overcoming Trastuzumab resistance caused by PTEN deficiency. *Clin Cancer Res.* 2007;13(19):5883.
- Meldal M, Tornøe CW. Cu-catalyzed Azide-alkyne cycloaddition. *Chem Rev.* 2008;108(8):2952–3015.
- Motzer RJ, Escudier B, Oudard S, Hutson TE, Porta C, Bracarda S, et al. Phase 3 trial of everolimus for metastatic renal cell carcinoma. *Cancer.* 2010;116(18):4256–65.
- Narayan M, Wilken JA, Harris LN, Baron AT, Kimbler KD, Maithe NJ. Trastuzumab-induced HER reprogramming in "resistant" breast carcinoma cells. *Cancer Res.* 2009;69(6):2191.
- Pergomet JL, Bracca ABJ, Kaufman TS. Total syntheses of gerberinol I and the pterophyllins 2 and 4 using the Casnati-Skattebøl reaction under different conditions. *Org Biomol Chem.* 2017;15(33):7040–9.
- Pretze M, Pietzsch D, Mamat C. Recent trends in bioorthogonal click-radiolabeling reactions using Fluorine-18. *Molecules.* 2013;18(7):8618–65.
- Sabatini DM. mTOR and cancer: insights into a complex relationship. *Nat Rev Cancer.* 2006;6(9):729–34.
- Salome C, Narbonne V, Ribeiro N, Thuaud F, Serova M, de Gramont A, et al. Benzofuran derivatives as a novel class of inhibitors of mTOR signaling. *Eur J Med Chem.* 2014a;74:41–9.
- Salome C, Ribeiro N, Chavagnan T, Thuaud F, Serova M, de Gramont A, et al. Benzofuran derivatives as anticancer inhibitors of mTOR signaling. *Eur J Med Chem.* 2014b;81:181–91.

- Tchevkina E, Komelkov A. Protein phosphorylation as a key mechanism of mTORC1/2 signaling pathways. In: Huang C, editor. Protein phosphorylation in human health: Online. London: IntechOpen; 2012. p. 3–50.
- Vinayak SMDMS, Carlson RWMD. mTOR inhibitors in the treatment of breast cancer. *Oncology*. 2013;27(1):38–44. 8 passim.
- Wander SA, Hennessy BT, Slingerland JM. Next-generation mTOR inhibitors in clinical oncology: how pathway complexity informs therapeutic strategy. *J Clin Invest*. 2011;121(4):1231–41.
- Yao JC, Fazio N, Singh S, Buzzoni R, Carnaghi C, Wolin E, et al. Everolimus for the treatment of advanced, non-functional neuroendocrine tumours of the lung or gastrointestinal tract (RADIANT-4): a randomised, placebo-controlled, phase 3 study. *Lancet*. 2016;387(10022):968–77.
- Yu K, Shi C, Toral-Barza L, Lucas J, Shor B, Kim JE, et al. Beyond Rapalog therapy: preclinical pharmacology and antitumor activity of WYE-125132, an ATP-competitive and specific inhibitor of mTORC1 and mTORC2. *Cancer Res*. 2010;70(2):621–31.
- Zhou H-Y, Huang S-L. Current development of the second generation of mTOR inhibitors as anticancer agents. *Chinese J Cancer*. 2012;31(1):8–18.

Publisher's Note

Springer Nature remains neutral with regard to jurisdictional claims in published maps and institutional affiliations.

Submit your manuscript to a SpringerOpen[®] journal and benefit from:

- ▶ Convenient online submission
- ▶ Rigorous peer review
- ▶ Open access: articles freely available online
- ▶ High visibility within the field
- ▶ Retaining the copyright to your article

Submit your next manuscript at ▶ [springeropen.com](https://www.springeropen.com)
